AD NUMBER
AD489200
LIMITATION CHANGES

TO:

Approved for public release; distribution is unlimited.
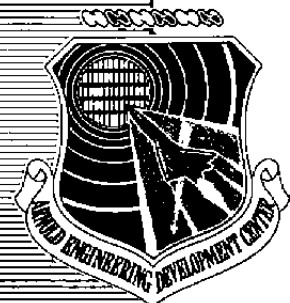
FROM:

Distribution authorized to U.S. Gov't. agencies and their contractors; Administrative/Operational Use; SEP 1966. Other requests shall be referred to Arnold Engineering Development Center, Arnold AFB, TN.

AUTHORITY

AEDC ltr 23 Jan 1975

OCT 14 1966

NOV 8 1966

$c_y 2$

AEROTHERMODYNAMIC CHARACTERISTICS
OF THE FULL-SCALE SNAP-27 VEHICLE AT
SUPERSONIC AND HYPERSONIC MACH NUMBERS

J. B. Carman, Jr.

ARO, Inc.

September 1966

VON KÁRMÁN GAS DYNAMICS FACILITY
ARNOLD ENGINEERING DEVELOPMENT CENTER
AIR FORCE SYSTEMS COMMAND
ARNOLD AIR FORCE STATION, TENNESSEE

NOTICES

AEROTHERMODYNAMIC CHARACTERISTICS
OF THE FULL-SCALE SNAP-27 VEHICLE AT
SUPERSONIC AND HYPERSONIC MACH NUMBERS

J. B. Carman, Jr.

ARO, Inc.

FOREWORD

The work reported herein was done at the request of the Atomic Energy Commission (AEC) for the General Electric Company (GE) under AEC SNAP-27 Program, AEC Activity No 04.30-01-41 3.

The results of the tests presented were obtained by ARO, Inc (a subsidiary of Sverdrup & Parcel and Associates, Inc.), contract operator of Arnold Engineering Development Center (AEDC), Air Force Systems Command (AFSC), Arnold Air Force Station, Tennessee, under Contract AF40(600)-1200. The test was conducted from April 11 to June 11, 1966, under ARO Project No. VT1674, and the manuscript was submitted for publication on August 3, 1966.

This technical report has been reviewed and is approved.

Donald E. Beitsch
Major, USAF
AF Representative, VKF
Directorate of Test

Leonard T. Glaser
Colonel, USAF
Director of Test

ABSTRACT

Heat-transfer, pressure, and static force tests were conducted at Mach 4 through 10 to obtain performance and design data on the SNAP-27 fuel cell. The tests were conducted using a full-scale model at free-stream unit Reynolds numbers between 0.6×10^6 and 5.0×10^6 per foot at angles of attack from -90 to 235 deg. Based upon early test results, the basic configuration was modified, successfully making the vehicle statically stable only at zero angle of attack at Mach 8. This was the only Mach number at which the modified configurations were tested.

CONTENTS

ILLUSTRATIONS

TABLE

NOMENCLATURE

b	Model skin thickness, ft
C_{A_T}	Total axial-force coefficient, axial force/$q_\infty S$
C_m	Pitching-moment coefficient, pitching moment/$q_\infty S\, D$
C_N	Normal-force coefficient, normal force/$q_\infty S$
c	Specific heat of model material, Btu/lb-°R
c_p	Specific heat of air at constant pressure, Btu/lb-°R
D	Reference length, model cylinder diameter, 4.00 in.
H	Enthalpy, Btu/lb
M	Mach number
p	Pressure, psia
q	Dynamic pressure, psia
$\dot{q}$	Local heat-transfer rate, Btu/ft^2-sec
Re	Unit Reynolds number, per foot
S	Reference area, model cylinder area, 12.56 in.^{2}
s	Distance along model circumference from nose, in.
St	Stanton number
T	Temperature, °R
t	Time, sec
u	Velocity, ft/sec
w	Model skin density, lb/ft^3
α	Angle of attack, deg
ρ	Density, lb/ft^3
ϕ	Roll angle, deg

SUBSCRIPTS

A	Model nose conditions at $\alpha = 0$
o	Tunnel stagnation conditions
w	Model wall conditions
∞	Free-stream conditions

SECTION I
INTRODUCTION

The SNAP-27 nuclear fuel cask, as the power generator for the Lunar Excursion Module, is to be landed on the moon where it must operate for one year in its lunar environment. In case of a mission abort resulting in an earth orbit, the SNAP-27 fuel cell must have the capability to re-enter the earth atmosphere intact to avoid radioactive contamination of the atmosphere. The objective of these tests was to provide experimental data to support the aerodynamic and thermodynamic design of the SNAP-27 configuration.

Force, pressure, and heat-transfer tests of a full-scale model of the SNAP-27 vehicle were conducted in the 40-in. supersonic tunnel (Gas Dynamic Wind Tunnel, Supersonic (A)) and the 50-in. hypersonic tunnels (Gas Dynamic Wind Tunnels, Hypersonic (B) and (C)) of the von Kármán Gas Dynamics Facility (VKF). Data were obtained at Mach numbers 4, 5, 6, 8, and 10 at Reynolds numbers between 0.6×10^6 and 5.0×10^6 per foot. Angle of attack varied from -90 to 235 deg.

SECTION II
APPARATUS

2.1 MODELS

Model photographs, details, and instrumentation are shown in Figs. 1, 2, and 3, respectively. The force and pressure models were machined from stainless steel, but the heat-transfer model was fabricated using a thin electroformed nickel shell. All models were furnished by the General Electric Company. For configuration clarity, various noses are defined by the letter N, bases by the letter B, and flaps by the letter F.

2.2 WIND TUNNELS

Tunnel A is a continuous, closed-circuit, variable density wind tunnel with an automatically driven flexible-plate nozzle and a 40- by 40-in. test section. The tunnel operates at Mach numbers from 1.5 to 6 at maximum stagnation temperatures up to 300°F ($M_\infty = 6$). Minimum operating pressures are about one-tenth of the maximum at each Mach number.

1

Tunnels B and C are continuous, closed-circuit, variable density wind tunnels with axisymmetric contoured nozzles and 50-in.-diam test sections. Tunnel B operates at a nominal Mach number of 6 or 8 at stagnation pressures from 20 to 280 and from 50 to 900 psia, respectively, at stagnation temperatures up to 1350°R. Tunnel C operates at a nominal Mach number of 10 at stagnation conditions from 200 to 2000 psia at 1900°R. The model may be injected into the tunnels for a test run and then retracted for model cooling or model changes without interrupting the tunnel flow. A description of the tunnels may be found in the Test Facilities Handbook.*

2.3 INSTRUMENTATION

Model forces and moments were measured with a six-component, moment-type, strain-gage balance supplied and calibrated by VKF. Before testing, combined balance static loadings were applied, simulating the model loading range anticipated during the test. The uncertainties listed below correspond to the differences between the applied loads and the values calculated by the final data reduction balance equations.

Balance Component	Design Load	Maximum Static Loads	Uncertainties
Normal force, lb	700	450	±1.5 lb
Pitching moment, in.-lb	3645	1730	±10 in.-lb
Axial force, lb	150	450	±1.0 lb

Pressures were measured using the standard pressure systems of Tunnels A and B. The Tunnel A system utilizes 15-psid transducers, referenced to a near vacuum, calibrated for ranges of 15, 5, and 1 psia. The precision of the system is estimated to have been within 0.2 percent of full scale of the range being used. Model pressures in Tunnel B were measured with 15-psid transducers, referenced to a near vacuum. From repeat calibrations, the estimated measurement precision was ±0.003 psia or ±0.5 percent, whichever was greater.

The heat-transfer model surface temperature was measured with thermocouples welded to the model inner surface. Thermocouple

---

*Test Facilities Handbook (5th Edition). "von Kármán Gas Dynamics Facility, Vol. 4." Arnold Engineering Development Center, July 1963.

outputs were recorded on magnetic tape, at a rate of 20 times per second, from the start of the injection cycle until about 3 sec after the model reached the tunnel centerline. From calibrations of typical thermocouple wires and a knowledge of the system sensitivity and noise level, the precision of the VKF temperature recording system is estimated to have been ±0.2°R/sec or ±2 percent, whichever was greater.

Model flow field schlieren photographs were obtained for the tests at Mach 6, 8, and 10. Figure 4 shows typical photographs at Mach 8.

SECTION III
PROCEDURE

3.1 TEST CONDITIONS

A summary of the configurations tested is given in Table I. The nominal tunnel conditions at which the tests were conducted are given below.

M_∞	P_o, psia	T_o, °R	$Re_\infty/ft \times 10^{-6}$
4	11 to 50	555	1.02 to 4.36
5	15 to 110	580 to 620	0.76 to 4.96
6	40 to 180	696 to 752	1.06 to 3.00
8	190 to 800	1240 to 1335	1.85 to 3.42
10	400 to 1400	1730 to 1875	0.58 to 1.70

3.2 DATA REDUCTION

Values of aerodynamic heating rate were calculated using temperature-time data in the relation

$$\dot{q} = wbc \frac{dT_w}{dt}$$

which neglects conduction and radiation losses. Stanton numbers were computed from the relation

$$St = \dot{q} / \left[\rho_\infty u_\infty \left(H_o - H_w \right) \right]$$

SECTION IV
RESULTS AND DISCUSSION

The Mach 10 longitudinal stability characteristics of two full-scale SNAP-27 configurations are presented in Fig. 5. As may be seen, no

Reynolds number effect was apparent on the basic configuration (N_1B_1). Also, the magnitudes of the normal-force, pitching-moment, and total axial-force coefficients for configuration N_1B_2 were slightly greater over the angle-of-attack range because of the larger flare. For both configurations, the peak in axial force near $\alpha = 147$ deg resulted when the bow wave from the vehicle base intersected the rear face of the nose. Although normal force was not affected, pitching moment was significantly increased, creating a stable trim point near $\alpha = 158$ deg. Both configurations were also stable at $\alpha = 0$ and 180 deg.

As the vehicle must re-enter the atmosphere with the nose heat shield windward to remain intact, elimination of the trim points at large angles was necessary. Figure 6 shows the stability characteristics of several modified vehicles at Mach 8, the only Mach number at which these modifications were investigated. The N_1B_1 data from Fig. 5, used as a reference, show that the combination Mach number-Reynolds number change did not significantly alter the stability characteristics of the basic configuration. The addition of a 3-in.-long flap to the base of the model $(N_1B_1F_2)$ eliminated the stable condition at $\alpha = 180$ deg, but only reduced the other trim angle from $\alpha = 158$ deg to near $\alpha = 147$ deg. However, by then modifying the nose $(N_2B_1F_2)$, all the large-angle stability conditions were eliminated. Extending the flap length to 5 in. $(N_1B_1F_3)$ accomplished the same result. A modification of the vehicle base proved undesirable, even using the most effective nose and base flap $(N_2B_3F_3)$. Stability characteristics near $\alpha = 0$ deg were not significantly altered by the vehicle modifications because all modified surfaces were located in regions of separated flow at low angles of attack.

Variation of stability characteristics with Mach number is shown in Fig. 7. As expected, normal-force, pitching-moment, and total axial-force coefficients decreased in magnitude with increasing Mach number. The appearance of the apparently double-valued pitching-moment and total axial-force coefficient data at Mach 4 is explained in Fig. 8.

At Mach 4, an intermittent flow occurred in the vehicle flow field between angles of attack of -3 and 3 deg. Flow behind the large blunted nose was at times partly attached, then fully separated as illustrated by the pressure distributions of Fig. 8. The flow variation affected pitching moment and axial force on the vehicle as might be expected. Fully separated flow reduced the magnitude of the axial force and pitching moment compared to the partly attached flow. However, for both flow conditions, the vehicle was statically stable at $\alpha = 0$ deg. Intermittent

flow conditions were also observed at Mach 5 and 6, but no evidence of this variation was observed at the higher Mach numbers (8 and 10) apparently because the flow was more capable of expanding into the cavity behind the blunt nose.

Typical pressure and heat-transfer distributions are presented in Fig. 9. In general, the peaks in both distributions were caused by shock wave interaction as seen in the schlieren photographs of Fig. 4.
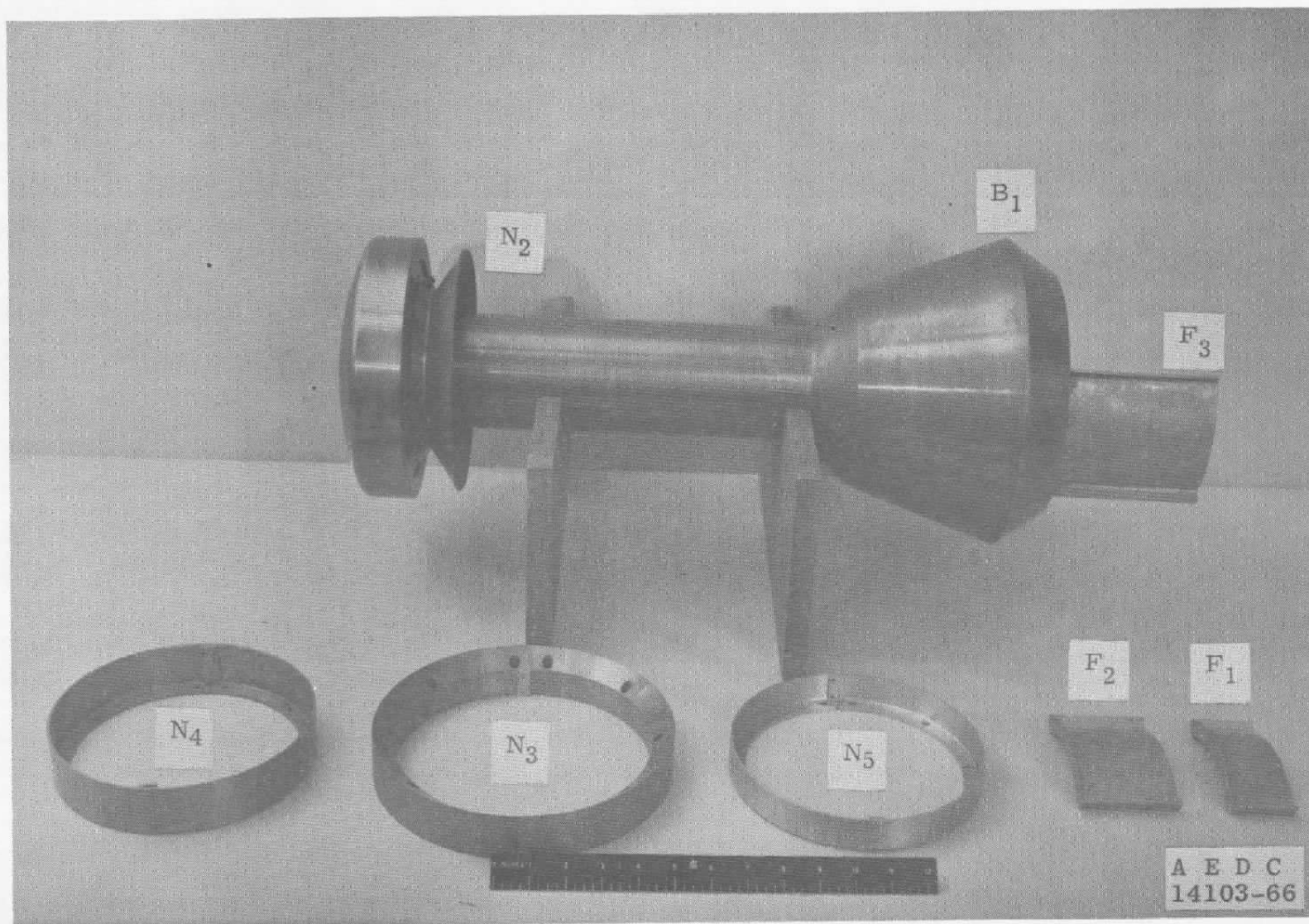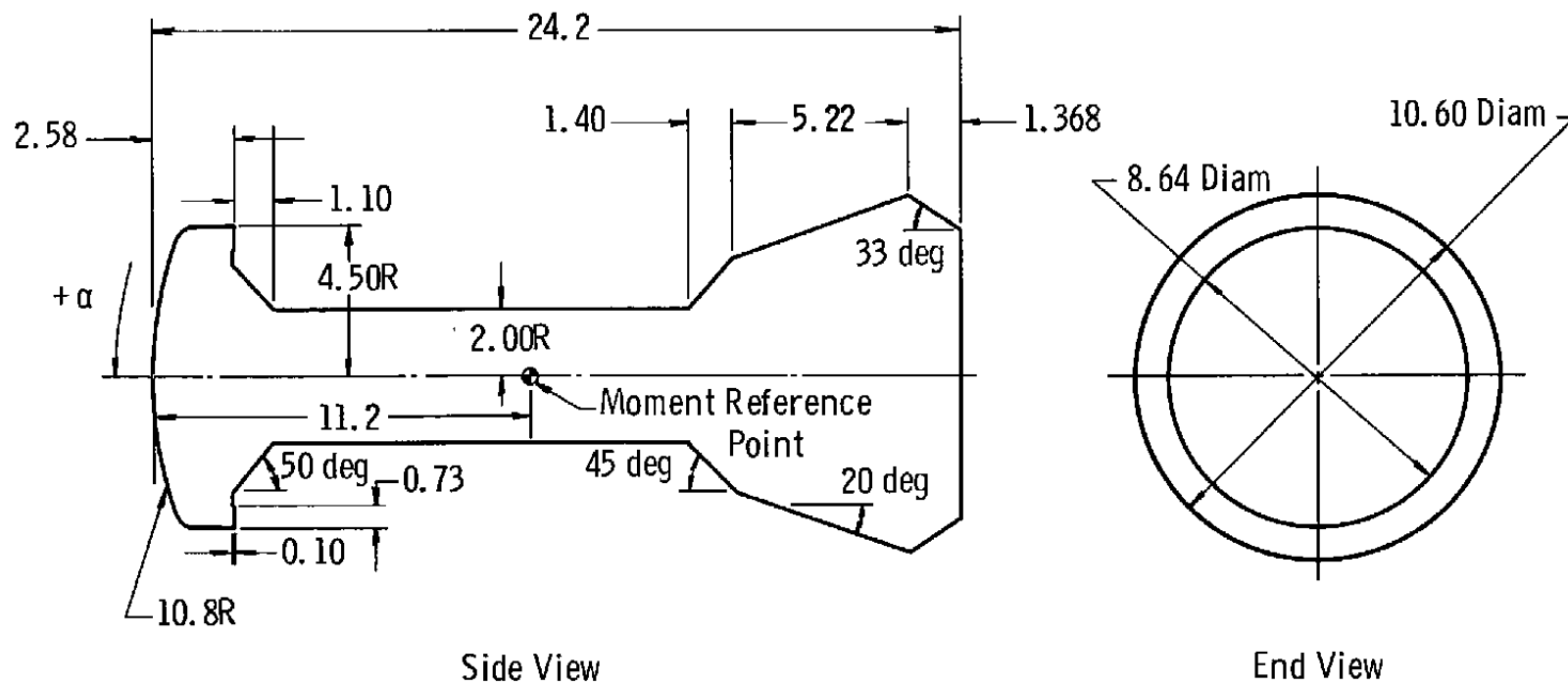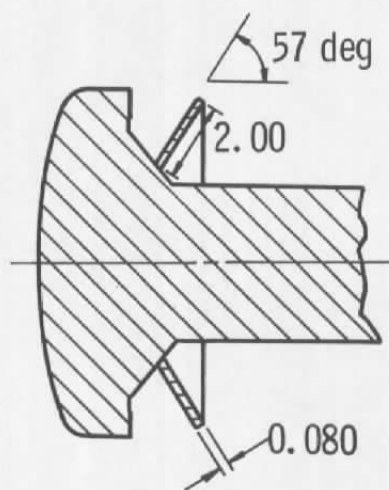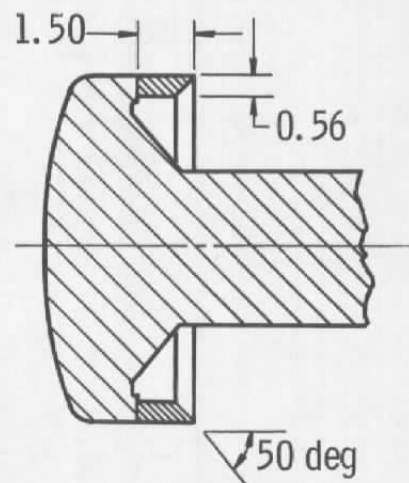
Fig. 1 Model Photograph

AEDC-TR-66-167

Side View

All Dimensions in Inches

a. Basic Configuration

Fig. 2 Model Details

57 deg

2.00

0.080

N_2

1.50

0.56

50 deg

N_3

1.50

0.080

N_4

1.00

0.080
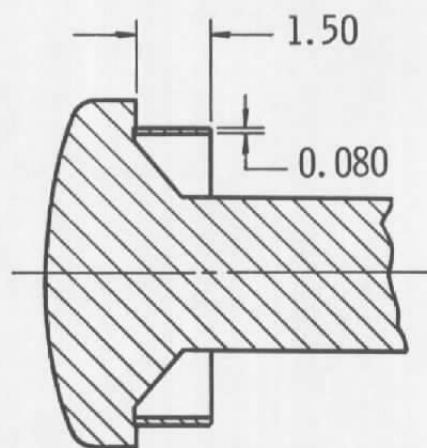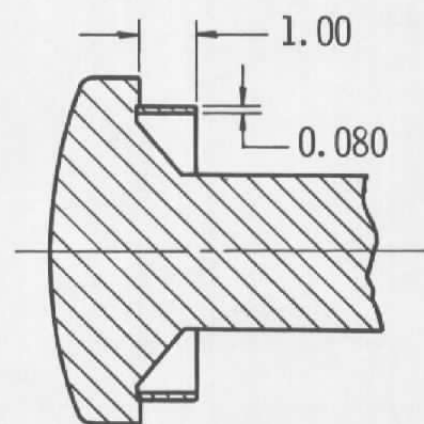
N_5

All Dimensions in Inches

b. Modified Nose Configurations

Fig. 2 Continued
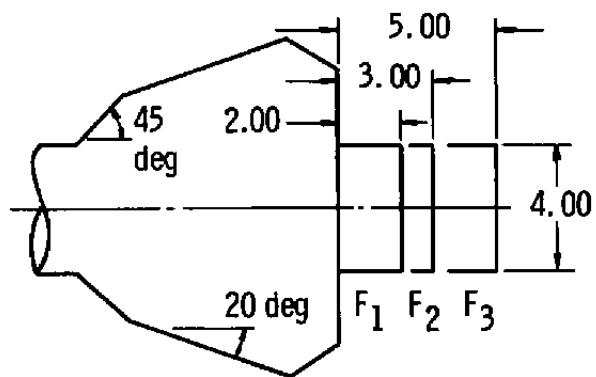
Top View
B_1 with Flaps
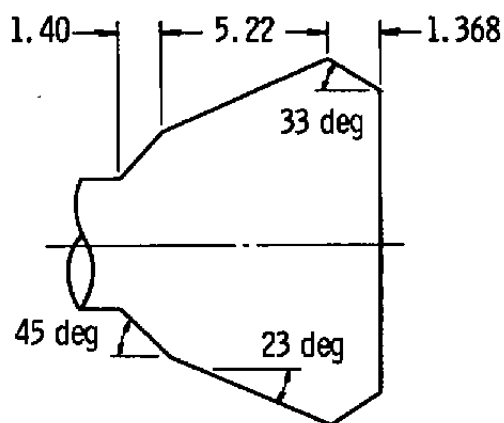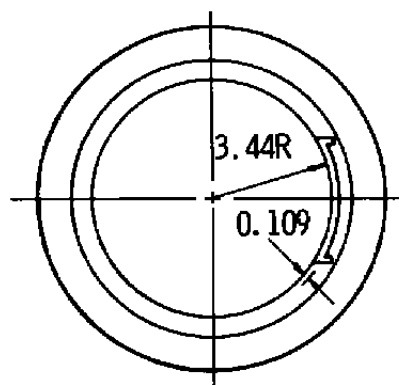
B_2
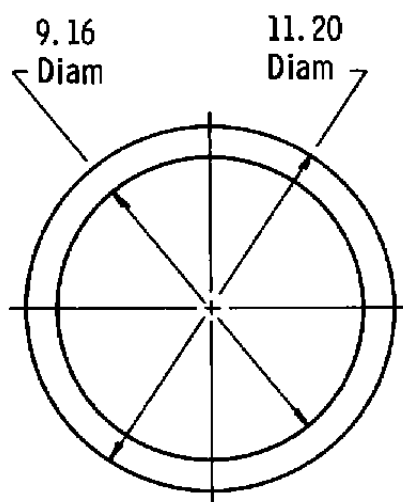
All Dimensions
in Inches
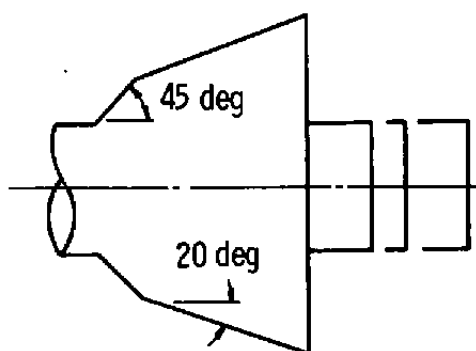
Top View
B_3 with Flaps
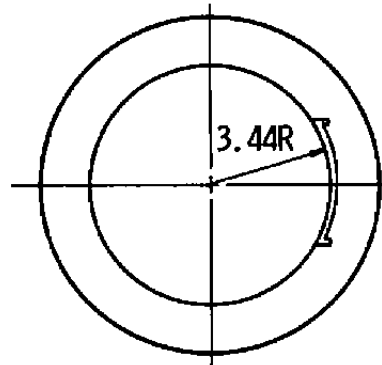
c. Modified Flare Configurations

Fig. 2 Concluded

180 deg

135 deg

Radial Station, in.

5 4 3 2 1

90 deg

0 deg

Front View

All Dimensions
in Inches

○ Pressure Port

0   4   8   12   16   20   24.2

Body Station, in.

Side View
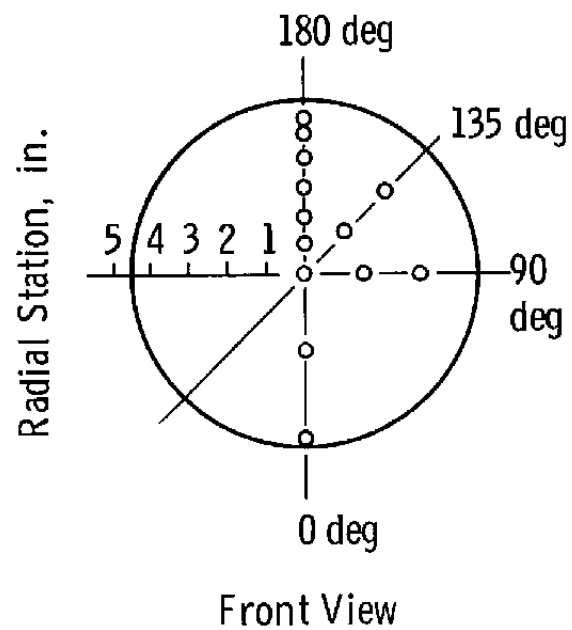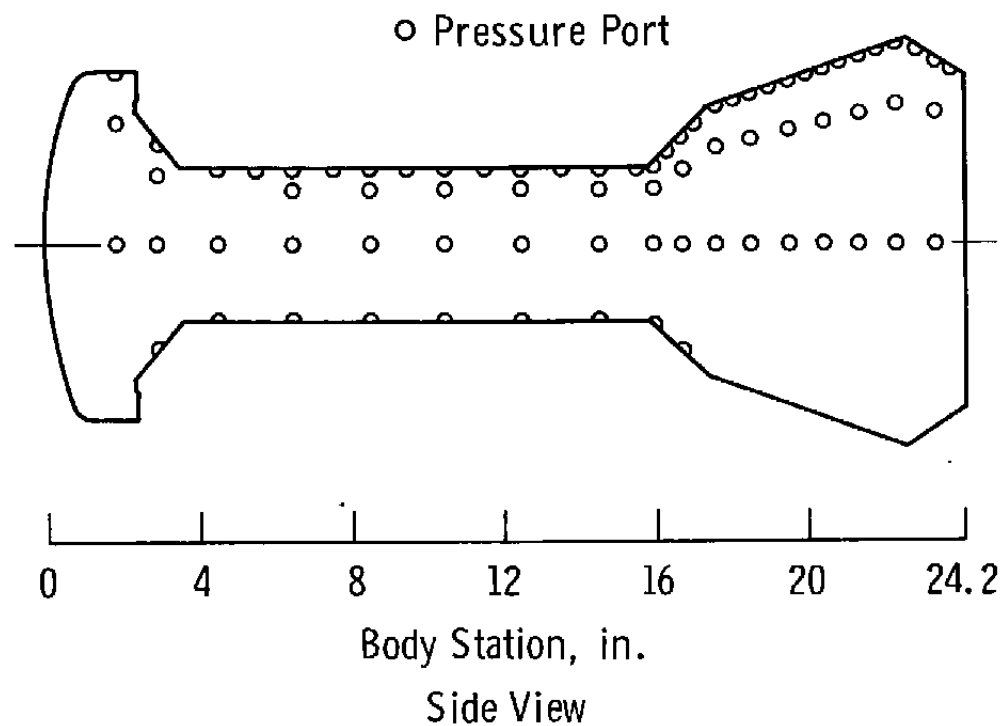
a. Pressure Model

Fig. 3 Model Instrumentation
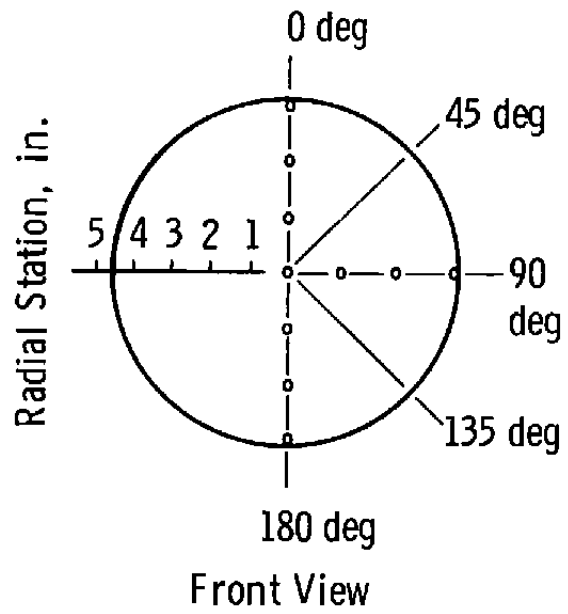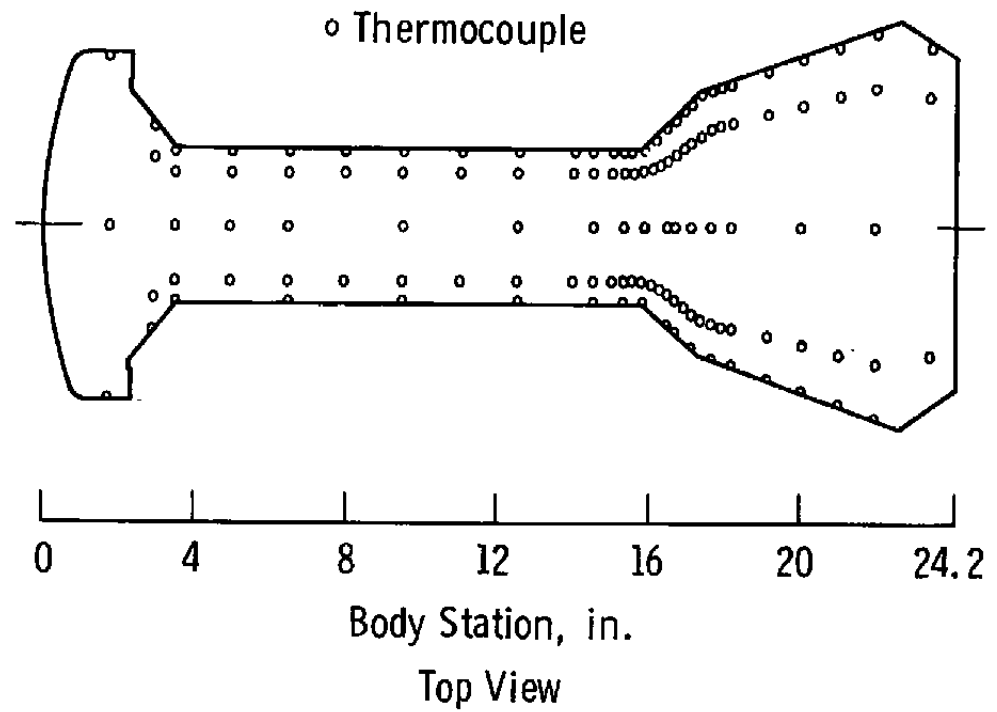
b. Heat-Transfer Model

Fig. 3 Concluded
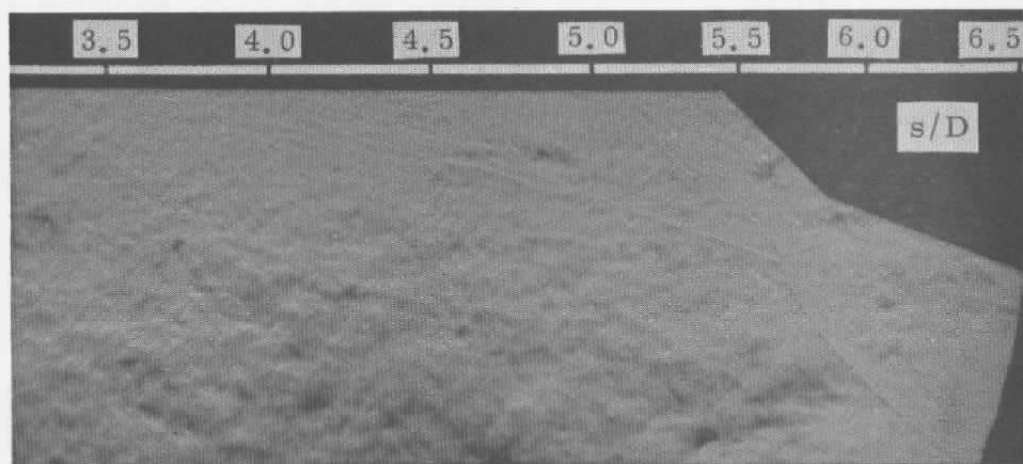
$\alpha = 0$ deg
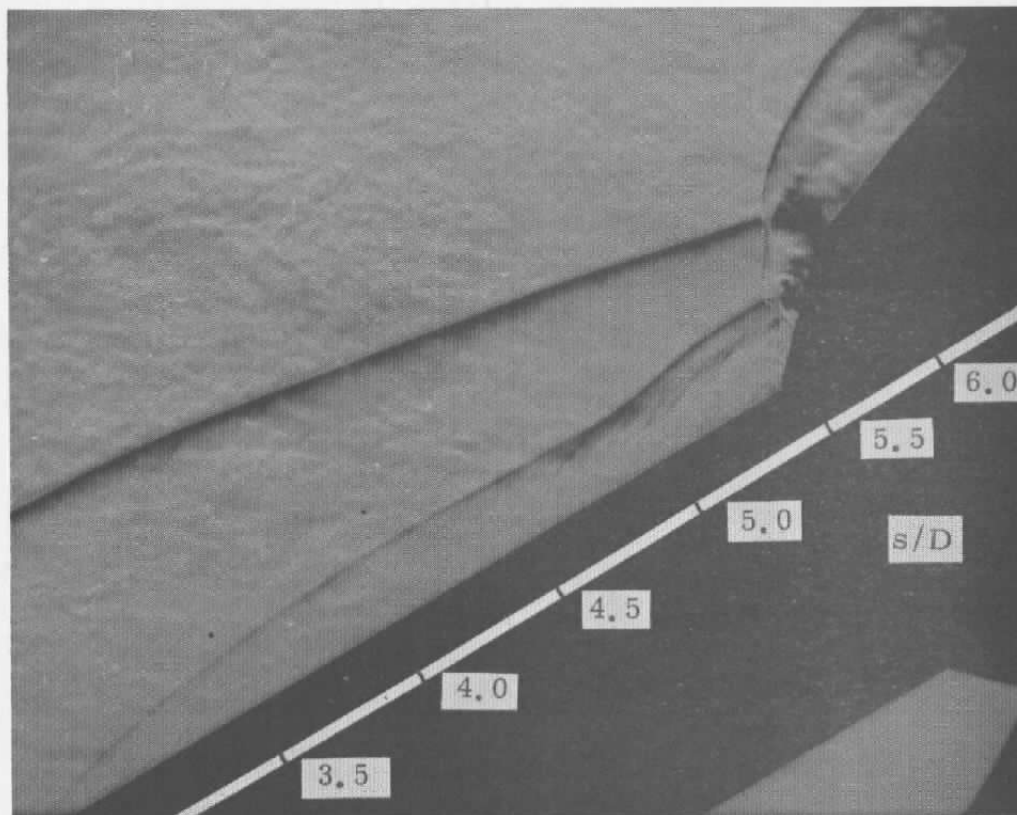
$\alpha = 30$ deg

Fig. 4 Typical Schlieren Photographs, $M_\infty = 8$, $Re_\infty = 3.4 \times 10^6$ per foot, Basic Configuration
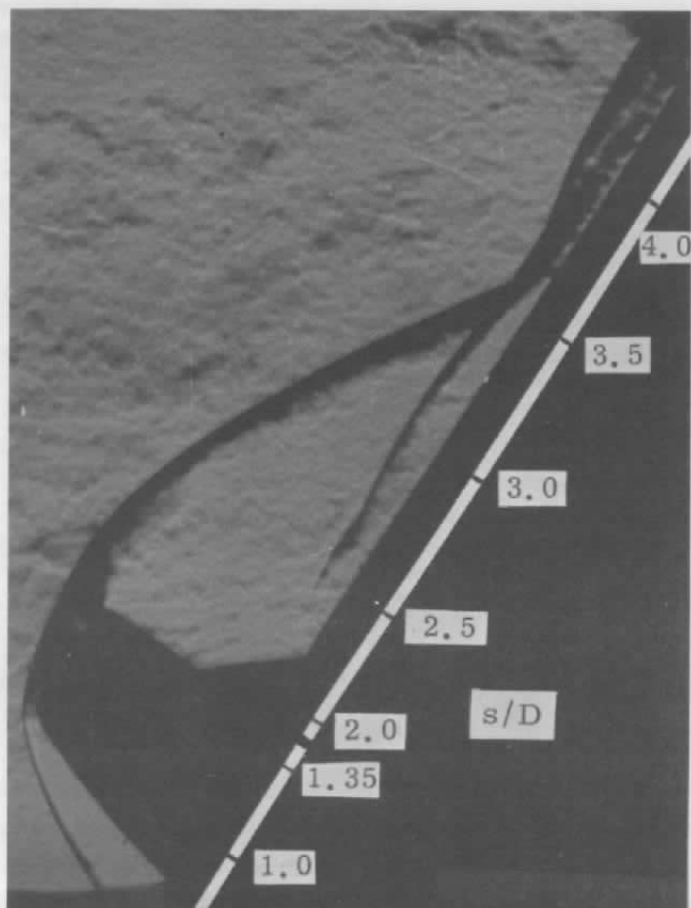
a = 55 deg
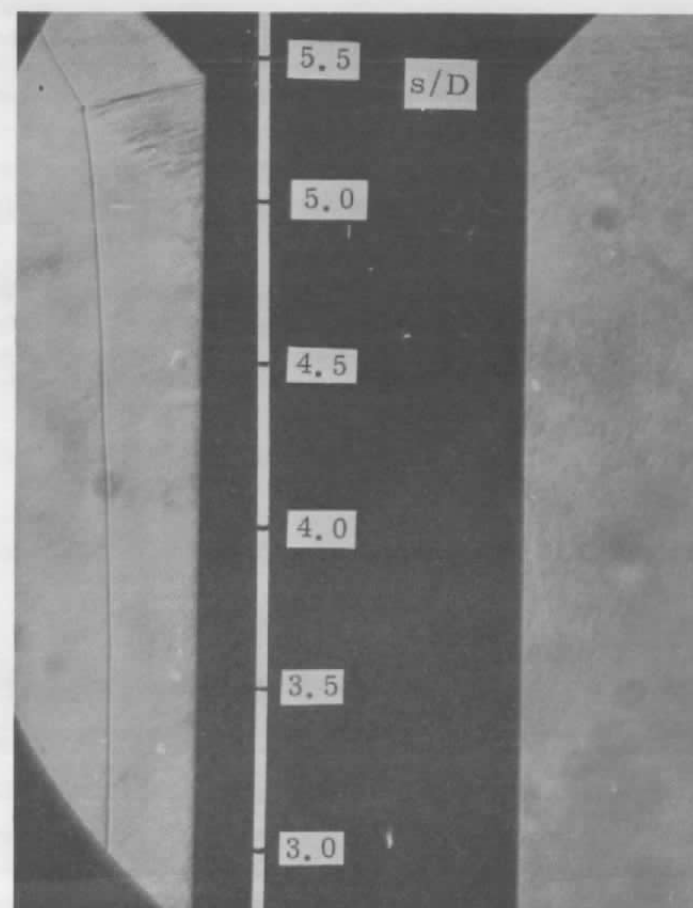
a = 90 deg

Fig. 4 Concluded
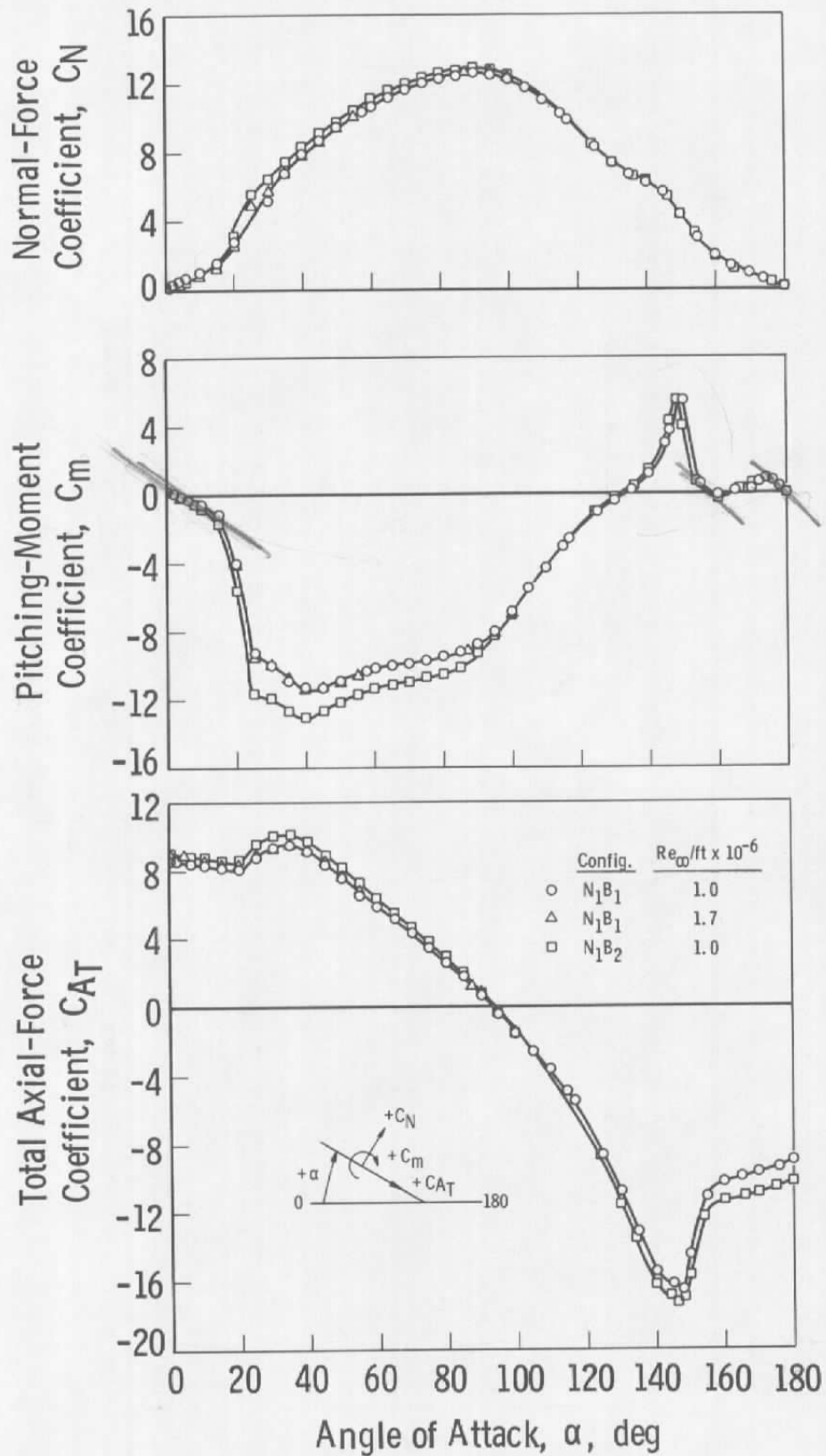
Fig. 5 Mach 10 Stability Characteristics

Config.	M_∞	$Re_\infty/ft \times 10^{-6}$
N_1B_1	10	1.0
N_1B_1	8	2.0
$N_1B_1F_2$	8	2.0
$N_1B_1F_3$	8	2.0
$N_2B_1F_2$	8	2.0
$N_2B_3F_3$	8	2.0
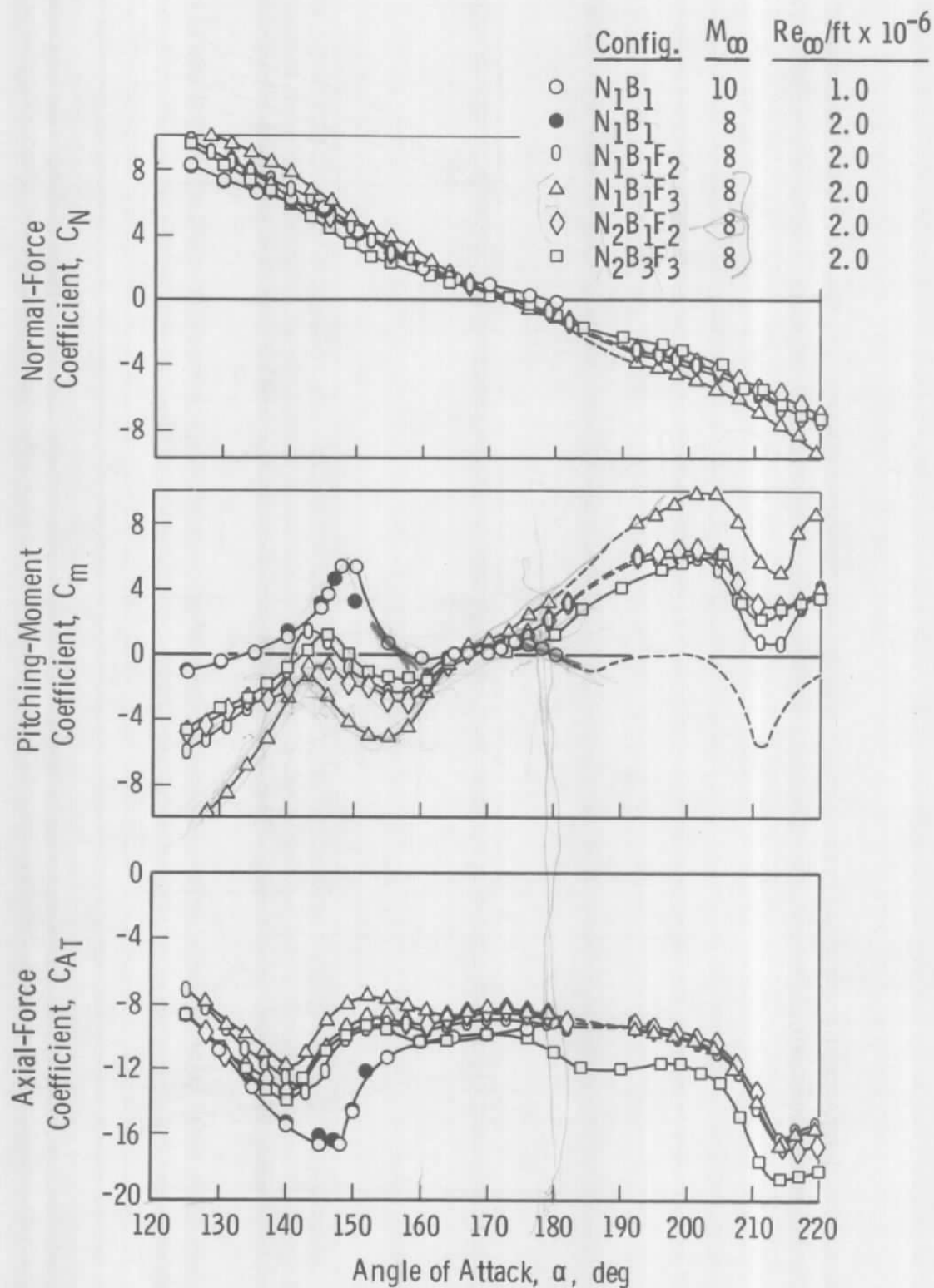
Fig. 6 Stability Characteristics of Several Modified Configurations
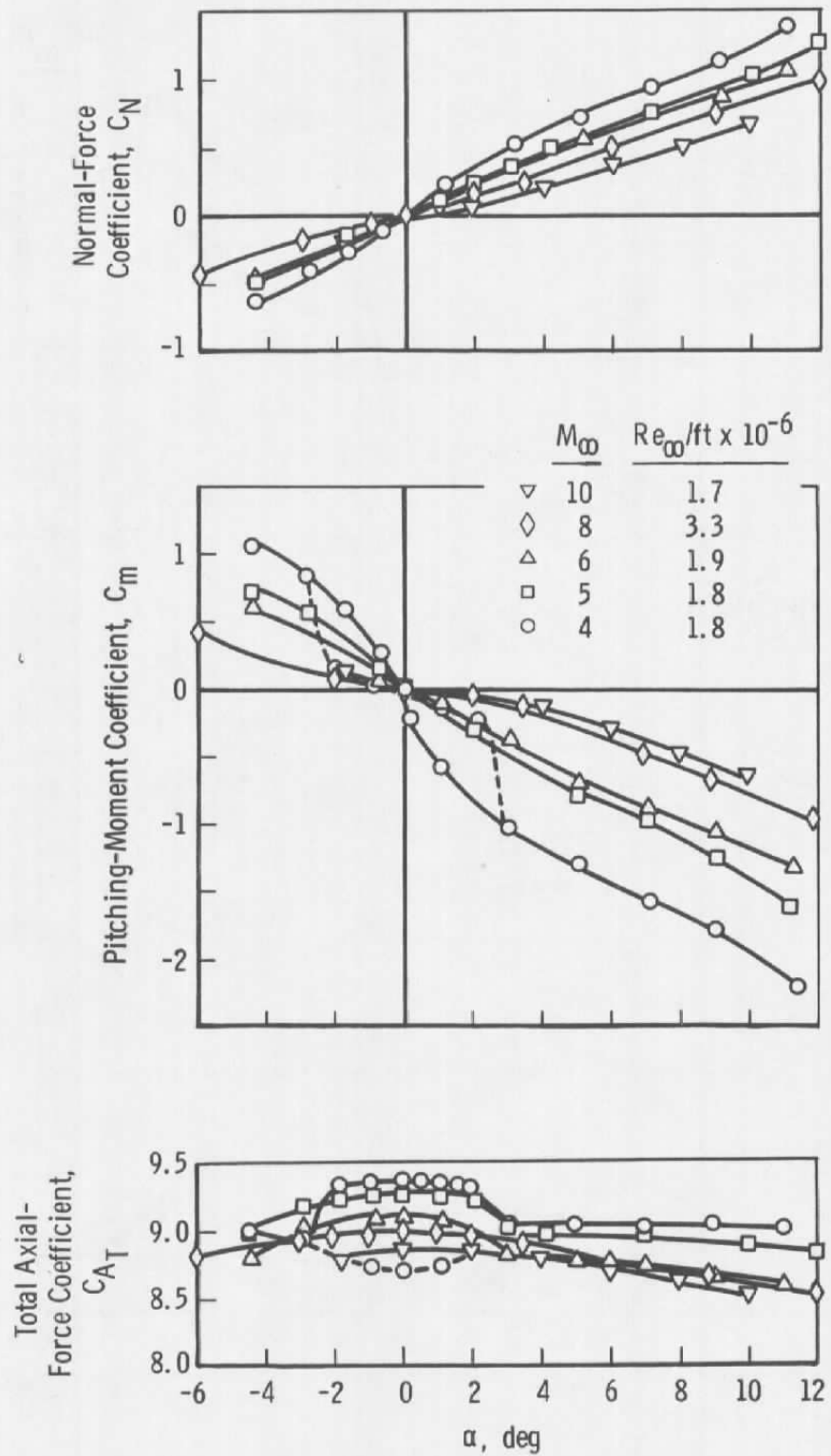
Fig. 7 Variation of Stability Characteristics with Mach Number, Basic Configuration
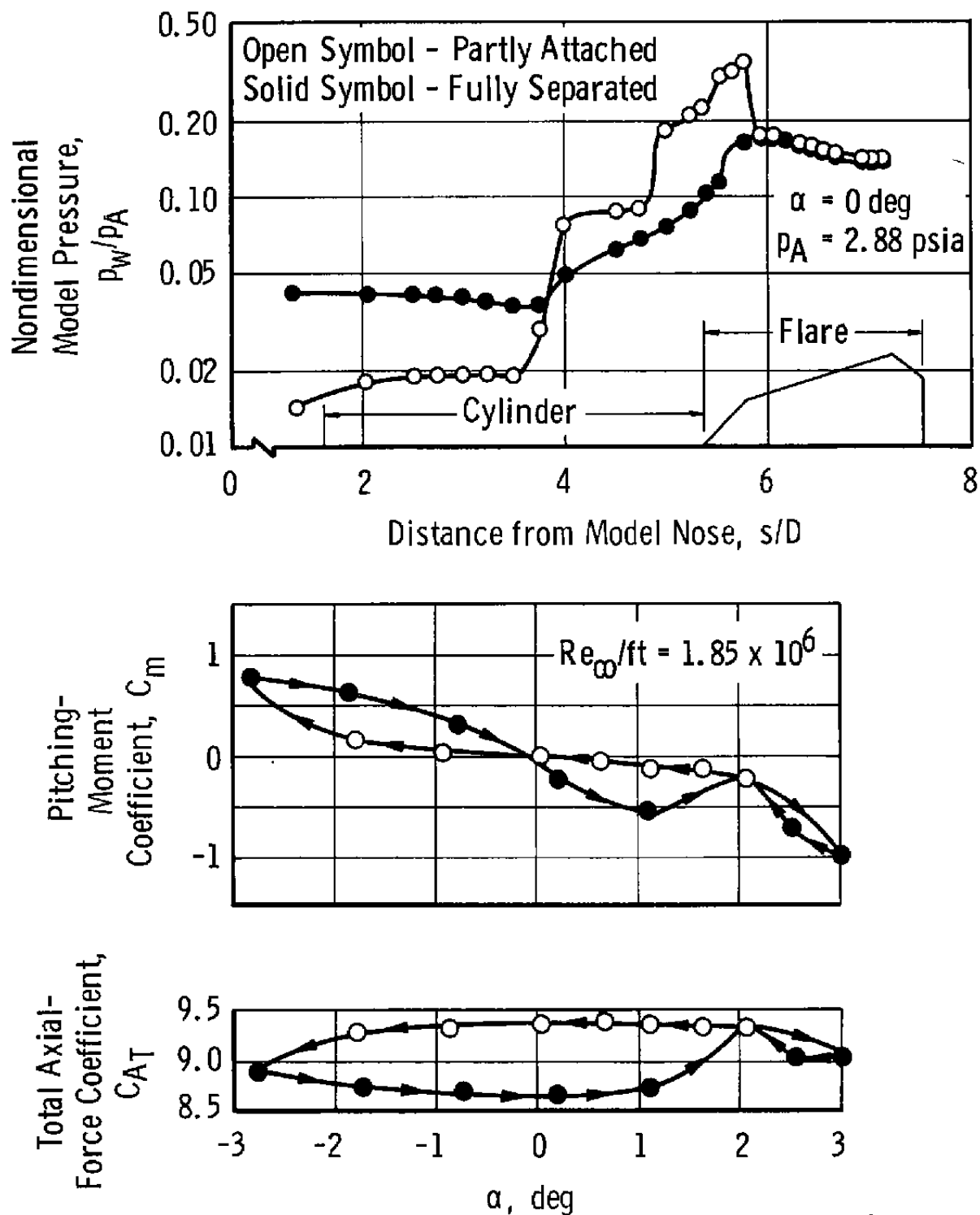
Fig. 8 Mach 4 Flow Field Instability, Basic Configuration
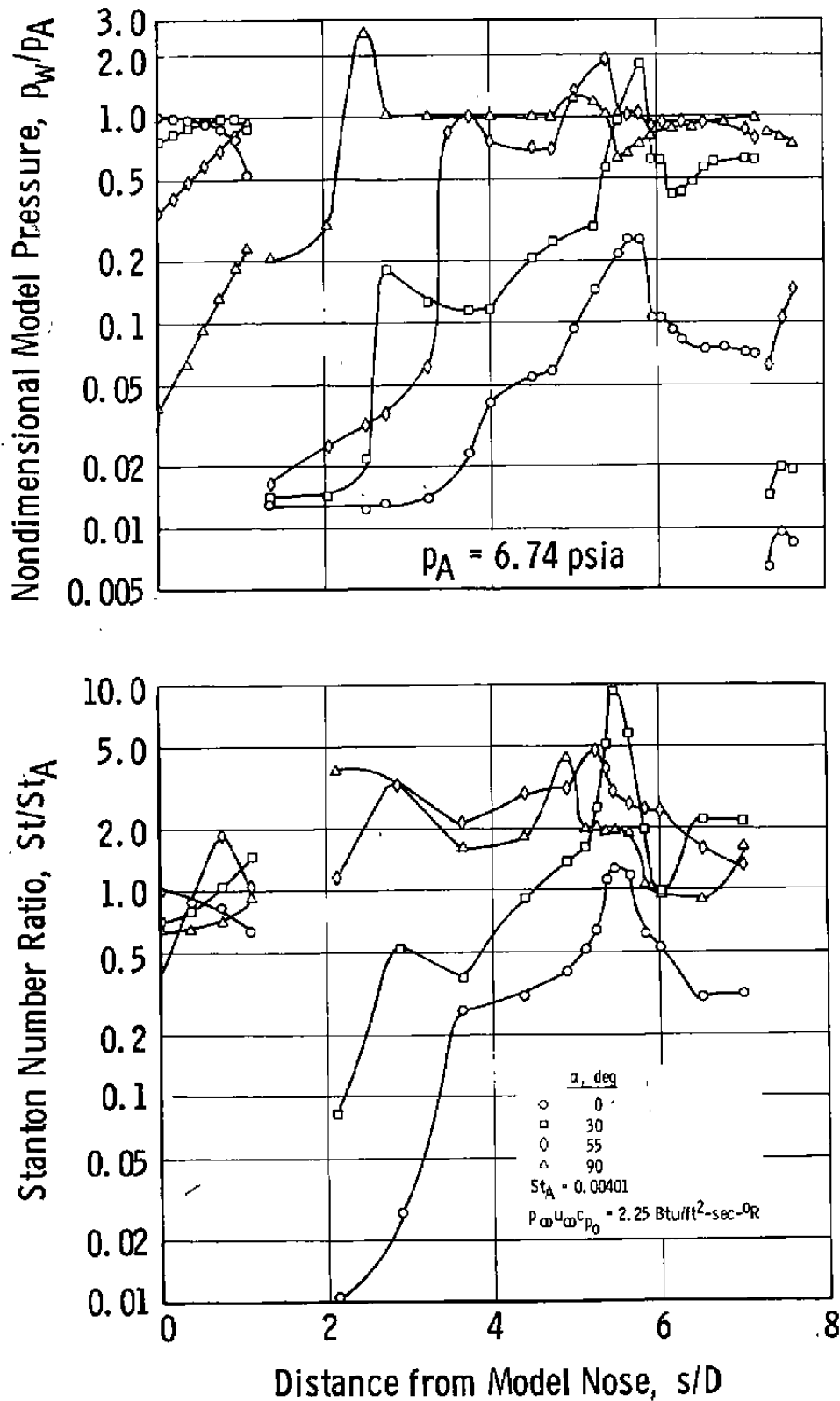
Fig. 9 Typical Mach 8 Pressure and Heat-Transfer Distributions, Re_∞ = 3.4 x 10^6 per foot, Windward Ray, Basic Configuration

TABLE I
TEST SUMMARY

M_∞	$Re_\infty/ft \times 10^6$	Configuration	ϕ, deg	α, deg	Data Type
4.02	4.31, 2.72	N_1B_1	0	-4.5 to 14.5	Static Stability
4.01	1.85				
3.99	1.02				
5.06	4.96, 2.75				
5.04	1.83				
5.03	0.76				
5.92	3.00				
5.90	1.90				
8.01	3.31	N_1B_1 $N_1B_1F_3$ $N_2B_1F_3$ $N_2B_3F_3$		-8 to 16	
7.97	1.87	N_1B_1, N_1B_3 N_2B_1, N_3B_1 N_4B_1		124 to 152	
	1.85	$N_1B_3F_3$		124 to 180	
		$N_2B_3F_3$		124 to 235	
		$N_1B_1F_2$		124 to 180 and 194 to 220	
		$N_1B_1F_3$ $N_2B_1F_1$ $N_2B_1F_2$			
		$N_1B_1F_3$	90	155 to 180	
		$N_2B_1F_2$ $N_2B_3F_3$			
10.08	1.00	N_1B_1, N_1B_2	0	0 to 180	
10.15	1.70	N_1B_1			
10.01	0.58			0 to 55 and 155 to 180	
4.02	4.36			-4.5 to 14.5	Pressure
4.01	1.85				
5.07	4.90			0 to 14 5	
5.86	1.06			-4.5 to 14.5	
5 91	1.91				
8.01	3 42			0 to 100	
7.98	2 15				
7.92	0.96				
8.01	3.42			-90 to 90	Heat Transfer
7.97	1.86				
7.92	1.01				

DOCUMENT CONTROL DATA - R&D

(Security classification of title, body of abstract and indexing annotation must be entered when the overall report is classified)

1 ORIGINATING ACTIVITY (Corporate author)	2a REPORT SECURITY CLASSIFICATION
Arnold Engineering Development Center ARO, Inc., Operating Contractor Arnold Air Force Station, Tennessee	UNCLASSIFIED
	2b GROUP N/A

3 REPORT TITLE

AEROTHERMODYNAMIC CHARACTERISTICS OF THE FULL-SCALE SNAP-27 VEHICLE AT SUPERSONIC AND HYPERSONIC MACH NUMBERS

4 DESCRIPTIVE NOTES *(Type of report and inclusive dates)*

N/A

5 AUTHOR(S) *(Last name, first name, initial)*

Carman, J. B., Jr., ARO, Inc.

6 REPORT DATE	7a TOTAL NO. OF PAGES	7b NO. OF REFS
September 1966	27	1

8a CONTRACT OR GRANT NO.	9a ORIGINATOR'S REPORT NUMBER(S)
AF 40(600)-1200	
b. AEC Activity No. 04.30-01-41.3	AEDC-TR-66-167
c	9b OTHER REPORT NO(S) *(Any other numbers that may be assigned this report)*
d	N/A

10 AVAILABILITY/LIMITATION NOTICES Qualified users may obtain copies of this report from DDC. Release to foreign nationals or foreign governments must have prior approval of AEC, Sandia Base.

11 SUPPLEMENTARY NOTES	12 SPONSORING MILITARY ACTIVITY
N/A	Atomic Energy Commission Sandia Base, Albuquerque, N.M.

13 ABSTRACT

Heat-transfer, pressure, and static force tests were conducted at Mach 4 through 10 to obtain performance and design data on the SNAP-27 fuel cell. The tests were conducted using a full-scale model at free-stream unit Reynolds numbers between 0.6×10^6 and 5.0×10^6 per foot at angles of attack from -90 to 235 deg. Based upon early test results, the basic configuration was modified, successfully making the vehicle statically stable only at zero angle of attack at Mach 8. This was the only Mach number at which the modified configurations were tested.

DD FORM 1 JAN 64 1473